

Evolutionary History of the Elliptical Galaxy NGC 1052

Michael Pierce^{1*}, Jean P. Brodie², Duncan A. Forbes¹, Michael A. Beasley^{1,2},
Robert Proctor¹, Jay Strader²

¹ Centre for Astrophysics & Supercomputing, Swinburne University, Hawthorn, VIC 3122, Australia

² Lick Observatory, University of California, Santa Cruz, CA 95064, USA

10 October 2018

ABSTRACT

We have obtained Keck spectra for 16 globular clusters (GCs) associated with the merger remnant elliptical NGC 1052, as well as a long-slit spectrum of the galaxy. We derive ages, metallicities and abundance ratios from simple stellar population models using the methods of Proctor & Sansom (2002), applied to extragalactic GCs for the first time. A number of GCs indicate the presence of strong blue horizontal branches which are not fully accounted for in the current stellar population models. We find all of the GCs to be ~ 13 Gyr old according to simple stellar populations, with a large range of metallicities. From the galaxy spectrum we find NGC 1052 to have a luminosity-weighted central age of ~ 2 Gyr and metallicity of $[\text{Fe}/\text{H}] \sim +0.6$. No strong gradients in either age or metallicity were found to the maximum radius measured ($0.3 r_e \simeq 1$ kpc). However, we do find a strong radial gradient in α -element abundance, which reaches a very high central value. The young central starburst age is consistent with the age inferred from the HI tidal tails and infalling gas of ~ 1 Gyr. Thus, although NGC 1052 shows substantial evidence for a recent merger and an associated starburst, it appears that the merger did not induce the formation of new GCs, perhaps suggesting that little recent star formation occurred. This interpretation is consistent with “frosting” models for early-type galaxy formation.

Key words: globular clusters: general – galaxies: individual: NGC 1052 – galaxies: star clusters.

1 INTRODUCTION

Globular clusters (GCs) are generally considered to be good tracers of a galaxy’s star formation history. Bimodal colour distributions are observed in many GC systems, suggesting that galaxies undergo multiple epochs of star and GC formation (Harris 2001). The exact nature of how these multiple star formation events occur is crucial to understanding galaxy formation.

Ashman & Zepf (1992) describe the production of metal-rich GCs during the merger of two gas-rich disc galaxies. This scenario results in similar ages for the metal-rich GCs and the merger event. In this model the blue, metal-poor GCs which belonged to the progenitor galaxies are universally old (~ 13 Gyr). Forbes, Brodie & Grillmair (1997) propose a multi-phase collapse, during which metal-poor GCs form early during the pre-galaxy collapse phase and, at a later time, metal-rich GCs form out of more enriched gas

at a similar time to the galaxy field stars. This model implies a metal-rich population that is a few Gyr younger than the metal-poor population. The exact age difference may depend on mass and environment (Beasley *et al.* 2002). On the other hand, Cote, Marzke & West (1998) suggest the bimodality of GC colours in large ellipticals is due to the gradual accretion of metal-poor GCs from dwarfs, with metal-rich GCs being indigenous to the elliptical. In this picture, the metallicity of the metal-rich population is a function of the galaxy’s luminosity and both sub-populations should be old.

These physical processes may all occur to some extent. To distinguish between the relative contributions of each process, we need examples of elliptical galaxies covering a range of masses and in different environments. Given that the above GC formation scenarios have different expectations concerning the ages of the metal-poor and metal-rich sub-populations, determining the age of individual GCs is a crucial step in testing these models.

There are several methods to measure GC properties such as age and metallicity from integrated spectra. Exam-

* mpierce@astro.swin.edu.au

ples include the method of Brodie & Huchra (1990; hereafter BH90), who present an empirical metallicity measure based on absorption line features. Another method is that of Strader & Brodie (2004; hereafter SB04), based on a principal components analysis (PCA) of 11 absorption line features. Methods involving spectral indices, predominantly the Lick system, and their comparison to simple stellar population (SSP) models can break the age-metallicity degeneracy (Worthey 1994). These methods usually rely on an age sensitive index (e.g., $H\beta$) and a metallicity sensitive index (e.g., Mgb) to break the degeneracy. However, these methods suffer difficulties when individual indices are contaminated, due to cosmic rays, skyline subtraction or galactic emission. Another complication is non-solar α -abundance ratios which are difficult to determine from index-index plots and can affect the higher order Balmer indices (Thomas, Maraston & Korn 2004). Recently, Proctor & Sansom (2002; hereafter PS02) have used a multi-index χ^2 -minimisation method to obtain ages, metallicities and abundance ratios for the stellar populations of late and early-type galaxies. Another advantage of using many indices is that it maximises the information used to break the age-metallicity degeneracy. Here we extend this method to extragalactic GCs for the first time (see Proctor, Forbes & Beasley 2004 for an application to Galactic GCs).

Hot luminous blue horizontal branch (BHB) stars have a significant effect on the measurement of several indices (most notably the Balmer indices, see Lee, Yoon & Lee 2000). Studies of Galactic GCs show that those with similar ages and metallicities can have very different spectral contributions from their HB stars depending on whether the HB stars are hot (blue) or cool (red). The way the HB is modelled has a significant impact on a SSP model (Maraston, Greggio & Thomas 2001a). A colour-magnitude diagram is probably the best way to deduce HB morphology in a given GC, but such diagrams are limited to GCs in the very nearest galaxies. Thus information on HBs in extragalactic GCs must generally come from integrated spectra. Old metal-rich GCs with BHBs (e.g., NGC 6388 and NGC 6441; Rich *et al.* 1997) can falsely appear to be intermediate-age clusters due to this strengthening of the Balmer lines (Schiavon *et al.* 2004), therefore, the ability to deduce HB morphology from integrated spectra is important. Schiavon *et al.* (2004) have recently introduced a method to detect anomalous HBs in GC spectra by differential comparisons of $H\delta$, $H\gamma$, and $H\beta$ line strengths.

There is evidence for a significant number of proto-GCs in galaxies which are currently merging (e.g., The Antennae; Whitmore & Schweizer 1995) and very recent (<500 Myr) mergers such as NGC 7252 (Maraston *et al.* 2001b; Schweizer & Seitzer 1998; Miller *et al.* 1997) and NGC 3921 (Schweizer, Seitzer & Brodie 2004; Schweizer *et al.* 1996). The outstanding questions are whether a substantial fraction of the proto-GC sub-population formed in these mergers survives, and hence whether it can account for the GC systems of ellipticals (see Forbes, Brodie & Grillmair 1997).

An important link between ongoing mergers and “old” elliptical galaxies is the intermediate aged (2-5 Gyr) merger remnants. Previous GC spectroscopic studies of merger remnant galaxies such as NGC 1316 (Goudfrooij *et al.* 2001) and NGC 3610 (Strader *et al.* 2003; Strader, Brodie & Forbes 2004) have confirmed a small number of GCs with

ages matching the time since the merger event (~ 3 Gyr and ~ 2 Gyr respectively). However, the total number of intermediate-age GCs in these galaxies is currently poorly constrained spectroscopically.

In this work we examine the GC system of NGC 1052, which is an excellent candidate for an elliptical that has undergone a minor merger event in the last few Gyr. NGC 1052 is an E4 galaxy, located in a small group at a distance of 18 Mpc (Forbes, Georgakakis & Brodie 2001b). Aside from containing an active nucleus, NGC 1052 displays several indications of a past merger or significant accretion event. The gas angular momentum is higher than that of the stellar component, with the gas and stars having different rotation axes (van Gorkom *et al.* 1986, Plana & Boulesteix 1996). NGC 1052 also reveals HI ‘tidal tails’ (van Gorkom *et al.* 1986), infalling HI gas onto the active nucleus (van Gorkom *et al.* 1989) and dust lanes (Forbes, Sparks & Macchetto 1990) all signs of an accretion or merger. van Gorkom *et al.* (1986) suggest that the HI observations could be explained by the accretion of a gas-rich dwarf, or other minor interaction, about 1 Gyr ago.

Despite the evidence for a recent accretion event, NGC 1052 shows almost no optical disturbance (it has a low fine structure value of $\Sigma = 1.78$, Schweizer & Seitzer 1992) and has a fundamental plane residual of $+0.07$ (Prugniel & Simien 1996) which is consistent with a normal galaxy on the fundamental plane (Forbes, Ponman & Brown 1998).

We can further probe the evolutionary history of NGC 1052 by measuring the ages and metallicities of individual GCs in the galaxy. The imaging of Forbes *et al.* (2001b) revealed a bimodal GC system as is typical for elliptical galaxies. The two sub-populations had a colour difference of $\Delta B-I=0.4\pm 0.1$. Using Worthey (1994) models, under the assumption that the blue GC sub-population is 15 Gyr old and metal-poor with $[Fe/H]=-1.5$, Forbes *et al.* (2001b) showed that any newly-formed red GCs (assuming ages of ≤ 2.5 Gyr) must have supersolar metallicities to fully account for the red sub-population.

In Section 2 we will present our observations and data reduction methods. Measured indices and our analysis of these Lick indices are given in Section 3. Using the method of PS02, metallicities, ages and abundance ratios are given in Section 4. Spectra of NGC 1052 itself are given in Section 5 and a brief analysis of GC kinematic data is in Section 6. Finally we discuss the implications of our results in Section 7 and present conclusions in Section 8.

2 OBSERVATIONS AND DATA REDUCTION

Spectra of GC candidates around NGC 1052 were obtained with the Low Resolution Imaging Spectrometer (LRIS; Oke *et al.* 1995) on the Keck I telescope. Candidate selection, based on the Keck imaging data of Forbes *et al.* (2001b), was designed to cover a wide range of potential GC colours (i.e. $1.2 < B-I < 2.5$, $0.6 < V-I < 1.7$). The properties of our candidates can be found in Table 1. Observations were obtained in 2003 January 25-27 with an integration time of $16 \times 1800s = 8$ hours for the slit-mask. However, the signal-to-noise ratios of the combined spectra were improved by excluding the exposures made at the highest airmass. These suffered from signal-to-noise degradation, especially at bluer

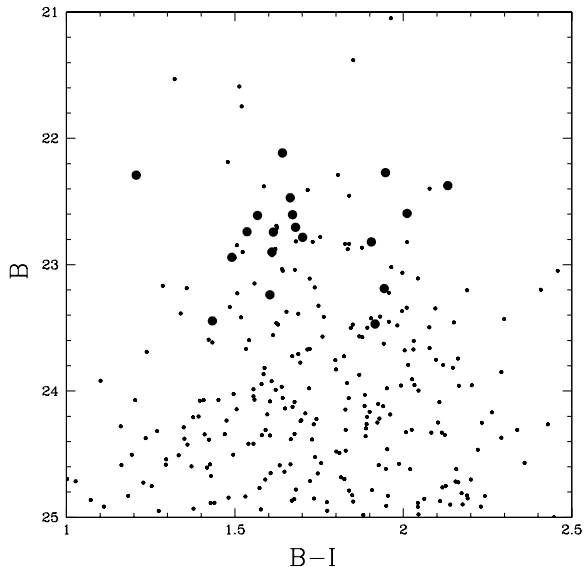


Figure 1. Candidate globular cluster colour magnitude distribution. GCs for which spectra were obtained are represented by large symbols. The small symbols are the full sample from the imaging study of Forbes *et al.* (2001b). Spectra were obtained for luminous GC candidates from both the blue and red sub-populations.

wavelengths. Seeing ranged between $0.65''$ and $0.75''$ over the three nights. A 600 lines per mm grating blazed at 4000 \AA was used for the blue side, resulting in an approximate wavelength range of $3300 - 5900 \text{ \AA}$ and a FWHM spectral resolution of $\sim 3.3 \text{ \AA}$.

Table 1 presents observational data for the objects for which we obtained Keck spectra. Figure 1, a B-I colour magnitude diagram, shows that we have obtained spectra from both the blue and red sub-populations of GC candidates. We have also generally sampled the most luminous GCs in NGC 1052. If any young (\sim few Gyrs old) GCs exist then they will tend to be brighter than the old population. Plotted in Figure 2 are the spatial positions of the confirmed GCs.

Data reduction was carried out using standard IRAF¹ methods. Tracing of spectra was done using the two exposures from each night with the lowest airmass (both < 1.2). These were combined to increase the signal for aperture tracing. They were then used as the reference apertures for their respective nights and spectra were extracted from individual exposures.

Comparison lamp spectra of Hg, Ar, Ne, Cd and Zn were used for wavelength calibration (mostly based on 8 Hg lines). Zero-point corrections of up to 3 \AA were performed on the science spectra using the bright OI skyline at 5577.34 \AA . Different methods of spectral combining were tested. Average combining was used with median scaled pixel rejection, due to the significant difference in flux levels between high and low airmass observations. Sigma clipping was used to

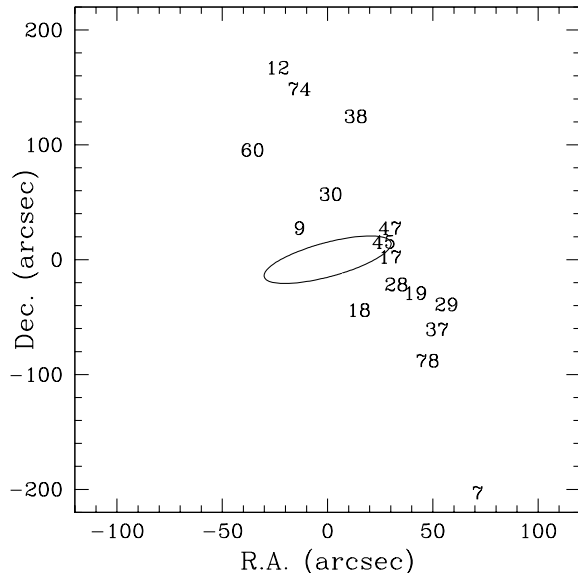


Figure 2. Spatial distribution of the confirmed GCs. The numbers correspond to the GCs listed in Table 1. The E4 ellipse represents the effective radius of NGC 1052 at $r_e \sim 34''$. The orientation is North up and East left. Note the x and y scales are different.

reject cosmic rays and reduce the effect of strong skylines. The resulting spectra have $S/N = 18-45 \text{ \AA}^{-1}$ measured at 5000 \AA .

Flux calibrations were provided by the flux standards Feige 34 and G191B2B. These were taken on the same run by long-slit and therefore have slightly different wavelength coverage to the multi-slit spectra. The velocities of GC candidates were determined by cross-correlation against high signal-to-noise M31 GC templates, i.e. 225–280 and 158–213 (see Beasley *et al.* 2004). The typical variation of V_{helio} with respect to the different templates is $\pm 20 \text{ km/s}$.

Of the 19 spectra obtained, one is a background galaxy with $z=0.204$, two are Galactic stars and the remaining 16 have velocities consistent with being GCs associated with NGC 1052. Thus, we have a success rate of 16 out of 19. Figure 3 shows the confirmed GC spectra smoothed to the Lick resolution. Each spectrum has been normalized, then offset by a flux interval of one, to make visual comparison easier. These spectra show a wide variation in the ratio of the CaII H and K features around 3950 \AA . Other prominent lines are the G band at 4300 \AA , H β (4863 \AA), Mg features (5200 \AA) and Fe lines around 5300 \AA .

3 GC SPECTRAL LINE INDICES

3.1 Measurement of Indices

We measured Lick indices (Trager *et al.* 1998; Worthey & Ottaviani 1997), the Rose (1984) CaII index, and BH90 indices from our flux-calibrated spectra after convolving the spectra with a wavelength-dependent Gaussian kernel to broaden to the Lick resolution. We then applied small offsets to the Lick indices based on measurements of several Lick standard stars (see Beasley *et al.* 2004). Uncertainties in the Lick indices were derived from the photon noise in

¹ IRAF is distributed by the National Optical Astronomy Observatories, which are operated by the Association of Universities for Research in Astronomy, Inc., under cooperative agreement with the National Science Foundation

Table 1. Globular Cluster candidates around NGC 1052. GC ID, R.A., Dec., V magnitude, B–I and V–I colours are from Forbes *et al.* (2001b). Galactocentric radii are calculated from GC positions assuming the distance to NGC 1052 of 18 Mpc. Heliocentric velocities are from this work.

ID	R.A.	Dec.	V	B–I	V–I	Radius	V_{helio}
GC	(J2000)	(J2000)	(mag)	(mag)	(mag)	(kpc)	(km/s)
GC7	02:41:00.0	-8:18:44.0	21.32	1.64	0.84	19.2	1659±74
GC9	02:41:05.7	-8:14:53.5	21.41	1.95	1.08	2.4	1649±105
GC11	02:41:00.2	-8:17:32.7	21.68	1.21	0.60	star
GC12	02:41:06.4	-8:12:33.9	21.40	2.13	1.16	14.2	1610±123
GC17	02:41:02.8	-8:15:18.6	21.72	1.66	0.92	1.9	1498±101
GC18	02:41:03.8	-8:16:04.9	21.71	2.01	1.13	4.3	1583±96
GC19	02:41:02.0	-8:15:50.1	21.85	1.67	0.92	4.7	1640±92
GC22	02:41:07.5	-8:13:13.1	21.87	1.68	0.85	star
GC28	02:41:02.6	-8:15:42.6	22.03	1.54	0.83	3.8	1414±86
GC29	02:41:01.0	-8:16:00.0	22.02	1.70	0.94	6.3	1273±78
GC30	02:41:04.7	-8:14:24.0	21.95	1.91	1.04	4.7	1537±122
GC37	02:41:01.3	-8:16:21.7	22.05	1.61	0.92	6.4	1443±76
GC38	02:41:03.9	-8:13:16.2	22.15	1.61	0.86	10.6	1295±122
GC45	02:41:03.0	-8:15:05.5	22.24	1.49	0.79	2.8	1765±74
GC47	02:41:02.8	-8:14:53.5	21.90	1.57	0.86	3.5	1781±83
GC55	02:41:00.8	-8:16:32.8	22.36	1.94	1.12	galaxy
GC60	02:41:07.2	-8:13:45.5	22.45	1.60	0.82	8.5	1415±122
GC74	02:41:05.7	-8:12:52.3	22.74	1.43	0.73	12.6	1675±93
GC78	02:41:01.6	-8:16:49.0	22.59	1.92	1.03	8.9	1619±92

the unfluxed spectra. Errors on the $H\beta$ index range from ± 0.21 – 0.36 Å. The Lick indices and Rose CaII index are presented for the confirmed GCs in Tables 2 and 3. We note that the 5202 Å skyline falls in the central band for Mg_2 and Mgb for our redshifted spectra, but in the Mgb side band for the Lick standard stars, raising some doubt over the accuracy of the offsets applied to the Mgb index and possible systematic errors in Mg_2 .

Missing values in Tables 2 and 3 indicate problematic indices due to various factors. Ionised gas emission from NGC 1052 has contaminated the $H\beta$ index in GCs 9 and 19. This can be seen clearly by examining the [OIII] emission feature at 5007 Å for GC19 in Figure 3. Difficulty subtracting the 5202 Å skyline from the Mg indices (especially Mgb) affects GCs 45, 60 and 74. The presence of some weak light from internal reflections within the LRIS instrument from the guide stars affects wavelengths below 4200 Å of GCs 12, 30, 45 and 60. Indices in parentheses are clipped from our fitting process due to their large deviance from the best fit age, metallicity and abundance ratio (see Section 3.3).

We have measured the BH90 indices, and using the method outlined in their paper, derived empirical metallicities. These values are obtained from an unweighted average of 6 metal-sensitive indices: CNB, G band, Fe52, MgH , Mg_2 and Δ (a measure of the 4000 Å break). The GCs affected by internal reflections do not have CNB or Δ included in their

BH metallicity estimate. Similarly, GCs with poor 5202 Å skyline subtraction do not have MgH or Mg_2 included. The GCs 45 and 60 are affected by both internal reflections and poor sky subtraction so their BH90 metallicities are based only on the Gband and Fe52. The final BH90 metallicity estimate is presented in Table 4. We also include in Table 4 the PCA metallicities derived using the method of SB04. PCA metallicity errors include only propagated errors in index measurement, not possible systematic errors in the metallicity relation itself (see SB04 for details).

3.2 Blue Horizontal Branches

Before estimating the ages and metallicities of the GCs from integrated spectra it is necessary to consider the effect of the horizontal branch morphology on the indices. Hot, luminous stars on the blue section of the horizontal branch of a GC can make a significant contribution to its spectrum (e.g., Lee, Yoon & Lee 2000). The effects of BHB stars are to both increase the intrinsic strength of the Balmer absorption lines and raise the blue continuum level, which in turn slightly increases the strength of all indices in the blue. This means that if the BHB of a GC is stronger than modelled, younger ages and higher metallicities (due to the age-metallicity degeneracy) are inferred. Current SSP models do not cover the full range of observed BHB morphology. For example,

Table 2. Globular Cluster indices $\lambda < 4500 \text{ \AA}$. Central index values (first line) and errors (second line). Indices in brackets are removed during the fitting process.

ID	CaII	H δ_A	H δ_F	CN ₁	CN ₂	Ca4227	G band	H γ_A	H γ_F	Fe4383	Ca4455
GC	ratio	(\AA)	(\AA)	(mag)	(mag)	(\AA)	(\AA)	(\AA)	(\AA)	(\AA)	(\AA)
GC7	1.01	2.07	2.60	(-0.039)	-0.038	(0.08)	(2.70)	-0.06	0.83	1.08	0.73
	0.07	0.33	0.21	0.010	0.012	0.19	0.34	0.35	0.22	0.52	0.27
GC9	1.41	0.06	0.70	(0.061)	(0.100)	1.19	(3.28)	-2.81	-0.15	3.72	1.00
	0.17	0.33	0.23	0.009	0.011	0.16	0.29	0.34	0.21	0.44	0.23
GC12	1.05	(0.86)	(4.07)	(-3.90)	(-1.04)	3.20	1.44
	0.10	0.17	0.30	0.35	0.22	0.47	0.24
GC17	0.94	2.81	2.20	(-0.057)	-0.050	(-0.33)	2.55	0.44	1.16	-1.16	1.24
	0.08	0.30	0.21	0.009	0.011	0.19	0.32	0.34	0.21	0.54	0.27
GC18	1.05	-2.05	-0.07	(0.010)	0.017	1.09	4.08	(-2.16)	(-0.03)	3.37	1.34
	0.13	0.41	0.27	0.011	0.013	0.21	0.36	0.42	0.26	0.57	0.28
GC19	1.17	2.79	(3.30)	(-0.024)	(0.020)	0.46	2.35	-0.36	1.30	1.40	0.21
	0.10	0.35	0.22	0.010	0.012	0.21	0.36	0.39	0.24	0.58	0.31
GC28	1.20	0.99	1.81	(0.029)	(0.049)	0.63	3.98	-3.01	-0.11	2.31	1.00
	0.15	0.39	0.25	0.011	0.013	0.21	0.38	0.42	0.26	0.62	0.31
GC29	0.96	1.83	(3.17)	-0.061	-0.022	(-0.22)	(1.26)	(-0.26)	1.21	2.66	1.12
	0.10	0.37	0.23	0.011	0.013	0.23	0.38	0.40	0.24	0.58	0.31
GC30	0.71	6.02	-4.99	-0.35	4.43	1.09
	0.21	0.34	0.44	0.26	0.55	0.30
GC37	0.94	2.23	1.89	(-0.071)	-0.056	0.63	1.99	-0.01	0.97	1.13	1.07
	0.11	0.39	0.27	0.011	0.014	0.21	0.41	0.41	0.25	0.63	0.32
GC38	0.78	3.68	3.01	(-0.089)	(-0.048)	-0.26	(1.45)	1.42	(1.40)	-1.13	0.50
	0.07	0.34	0.23	0.010	0.012	0.22	0.38	0.38	0.24	0.62	0.32
GC45	1.14	(-0.03)	(2.58)	3.02	2.72	-0.33	0.64
	0.12	0.29	0.48	0.47	0.29	0.68	0.35
GC47	1.13	-2.53	-0.11	(0.102)	0.104	(-0.39)	(3.59)	(-2.23)	(0.69)	4.48	1.48
	0.13	0.40	0.26	0.010	0.013	0.20	0.36	0.39	0.23	0.52	0.28
GC60	0.84	(-1.02)	(3.79)	0.49	1.81	0.27	(-1.58)
	0.10	0.27	0.41	0.44	0.27	0.71	0.38
GC74	0.81	3.98	(2.40)	-0.107	-0.083	0.36	0.27	2.55	1.96	1.94	0.61
	0.09	0.41	0.29	0.013	0.015	0.25	0.48	0.46	0.28	0.73	0.39
GC78	1.09	-0.03	1.21	-0.009	0.011	0.67	(-0.72)	(0.84)	(1.46)	2.31	0.13
	0.15	0.50	0.33	0.014	0.017	0.27	0.53	0.51	0.31	0.77	0.42

Bruzual & Charlot (2003) SSPs incorporate the effect of a blue HB population for metal-poor GCs. Thomas, Maraston & Bender (2003; hereafter TMB03) allow a choice of a blue horizontal branch (BHB) or red horizontal branch (RHB) for old metal-poor populations, although this only applies to the Balmer indices. Thomas, Maraston & Korn (2004; hereafter TMK04) include BHB morphology for the old, metal-poor regime changing to RHB morphology in the

metal-rich regime. We will show that anomalously blue HBs are likely present in several of our GCs.

One indicator for the presence of BHB stars in old populations is the Rose (1984) CaII index (Trippico 1989). The CaII index is defined as the ratio of the central intensity of CaII H + He ϵ at 3968 \AA divided by the central intensity of CaII K at 3933 \AA . The BHB stars greatly increase the absorption of He and therefore lower the value of this ratio

Table 3. Globular Cluster indices $\lambda > 4500$ Å. Central index values (first line) and errors (second line). Indices in brackets are removed during the fitting process.

ID	Fe4531	C4668	H β	Fe5015	Mg ₁	Mg ₂	Mgb	Fe5270	Fe5335	Fe5406
GC	(Å)	(Å)	(Å)	(Å)	(mag)	(mag)	(Å)	(Å)	(Å)	(Å)
GC7	(2.84)	1.34	2.50	3.10	(0.012)	(0.074)	(0.98)	1.46	1.46	0.94
	0.42	0.65	0.24	0.53	0.005	0.006	0.25	0.27	0.31	0.23
GC9	2.74	1.19	3.33	0.062	(0.182)	2.80	2.14	(0.76)	1.26
	0.35	0.54	0.45	0.004	0.005	0.21	0.23	0.26	0.19
GC12	3.30	3.15	1.76	4.93	0.085	(0.235)	3.56	2.02	1.97	1.05
	0.36	0.57	0.22	0.47	0.005	0.006	0.22	0.24	0.27	0.20
GC17	2.61	(-2.46)	2.34	(0.31)	(0.043)	0.089	0.91	0.42	(-0.55)	0.62
	0.41	0.67	0.25	0.56	0.006	0.006	0.27	0.30	0.34	0.24
GC18	2.61	2.62	(2.34)	3.78	0.087	(0.257)	3.32	(2.87)	1.27	0.64
	0.44	0.66	0.25	0.55	0.006	0.006	0.25	0.28	0.31	0.23
GC19	2.23	0.72	1.53	(0.058)	0.072	1.10	1.31	0.18	0.47
	0.46	0.72	0.62	0.006	0.007	0.29	0.32	0.37	0.26
GC28	2.25	(2.68)	2.17	(2.42)	0.062	(0.125)	1.93	2.55	(0.48)	1.22
	0.48	0.74	0.28	0.64	0.006	0.007	0.30	0.33	0.38	0.27
GC29	1.97	(2.35)	(2.81)	2.67	0.073	0.134	2.03	1.11	2.16	0.78
	0.48	0.74	0.28	0.64	0.007	0.008	0.30	0.34	0.39	0.28
GC30	2.56	2.75	2.40	3.94	0.090	0.197	2.60	1.78	(0.62)	0.68
	0.45	0.70	0.27	0.59	0.006	0.007	0.28	0.31	0.36	0.26
GC37	1.49	0.32	2.03	2.61	(0.066)	0.121	1.24	(1.97)	1.16	0.95
	0.50	0.77	0.29	0.64	0.006	0.007	0.30	0.33	0.37	0.27
GC38	1.07	(1.58)	2.95	(2.61)	0.006	(0.091)	1.03	1.19	-0.63	0.49
	0.50	0.77	0.29	0.66	0.007	0.008	0.32	0.36	0.43	0.30
GC45	1.38	(-2.02)	1.97	(5.98)	(0.104)	(0.144)	1.08	(2.91)	0.01
	0.58	0.88	0.35	0.75	0.008	0.009	0.40	0.45	0.32
GC47	(1.62)	(0.07)	1.26	5.92	0.114	0.239	3.46	2.92	1.91	1.38
	0.43	0.65	0.26	0.55	0.006	0.007	0.25	0.28	0.32	0.23
GC60	0.30	(2.68)	(2.36)	1.92	(0.040)	0.059	(2.07)	1.10	(1.09)
	0.57	0.83	0.31	0.71	0.007	0.008	0.36	0.41	0.29
GC74	-0.62	0.24	3.64	-0.67	0.034	0.050	1.09	0.01	0.10
	0.64	0.96	0.34	0.85	0.008	0.010	0.44	0.51	0.37
GC78	2.02	1.19	2.30	3.19	0.045	0.144	1.78	2.75	1.91	1.27
	0.63	0.96	0.36	0.79	0.008	0.009	0.38	0.40	0.45	0.33

(young GCs might be expected to show a similar behavior). This effect, known as the “Ca Inversion”, can be clearly seen in GCs such as GC74 and GC38 of our sample (see Figure 3), which have CaII index values of 0.81 and 0.78 respectively. Our CaII indices are presented in Table 2 (we were unable to measure the CaII index for GC30). Although reflections may effect the measurement of the CaII index in some GCs, the lines are sufficiently strong so that the effect

is minor. The CaII indices are plotted in Figure 4 against BH90 metallicities. This figure shows that, as expected, GCs with BHBs tend to be metal-poor.

Problems occur with fitting the indices to SSP models when the observed GC has a BHB contribution significantly greater than is modelled or when BHBs are present in metal-rich GCs (i.e. $[\text{Fe}/\text{H}] > -1.0$). Another difficulty arises for the

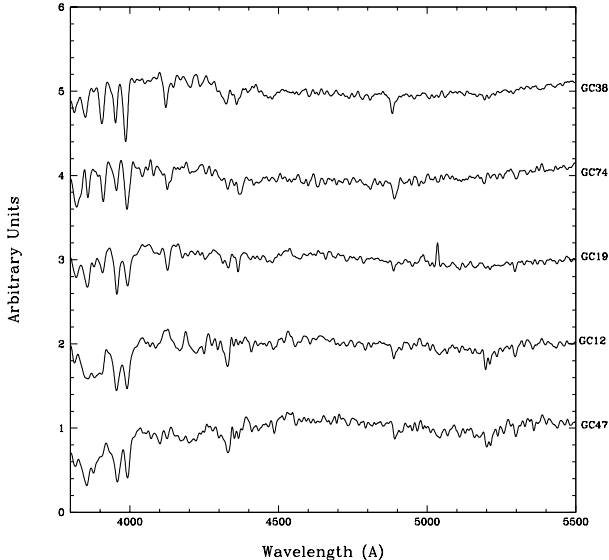


Figure 3. Selected Keck spectra of NGC 1052 GCs normalized and offset by 1 unit. These spectra have not been de-redshifted (which introduces a shift of ~ 25 Å). The spectra show the strong CaII H and K features around 3950 Å, the Gband at 4300 Å, H β (4863 Å), Mg feature (5200 Å), Fe lines around 5300 Å and other absorption lines. The emission line at ~ 5035 Å in GC19 is [OIII]5007 Å from the galaxy which did not fully subtract. The spectra indicate a range of metallicities and CaII ratios.

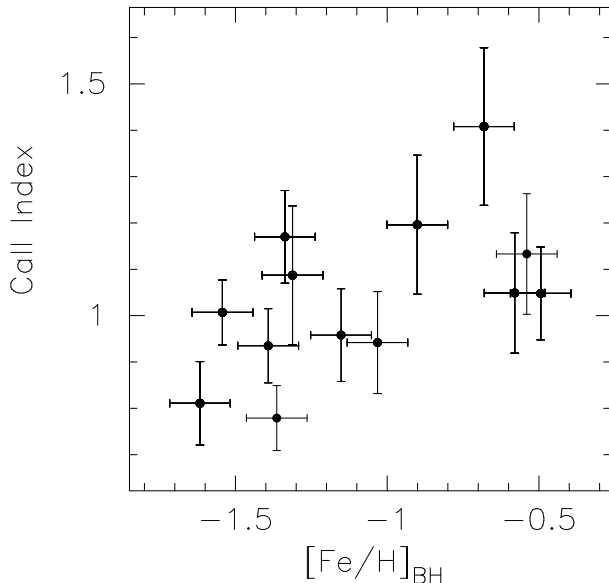


Figure 4. The CaII index against BH90 metallicity. There is a trend for low CaII values (indicating the presence of a blue horizontal branch) to be found in metal-poor globular clusters. The $[\text{Fe}/\text{H}]_{\text{BH}}$ errors are indicative only. GCs 45 and 60 are not plotted because their BH90 metallicities are based on only two indices.

case of metal-poor GCs with RHBs. Only the TMB03 SSP models cover this situation.

3.3 Fitting Indices to Simple Stellar Population Models

Ages and metallicities are derived by comparing the measured indices with SSP models. The choice of which SSP model to use is not obvious since all the models have different advantages and limitations. We decided to use the recent models of TMK04, who modelled the affect of abundance ratios on the H γ and H δ Balmer lines for the first time. These models only differ significantly from TMB03 at high metallicity (i.e. $[\text{Fe}/\text{H}] > -0.35$). We have also examined Vazdekis (1999), Bruzual & Charlot (2003) and TMB03 SSP models and find qualitatively similar results for the derived ages, metallicities and abundance ratios ($[\text{E}/\text{Fe}]$). For a comparison of SSP models see Proctor *et al.* (2004).

To derive accurate measures of GC parameters, particularly in view of the problematic indices discussed in Section 3.1, we need to include as many reliable indices as possible in the fitting process. Here, we use all uncontaminated indices in a multi-dimensional fitting procedure (see PS02), using the SSP models of TMK04, which include α -enhancement. A χ^2 -minimisation fit is made to the SSP grid points, including an interpolation along all three parameter axes.

We reject outliers by iteratively excluding the index that has the greatest contribution to the overall χ^2 . This decision is based not only on the individual index's χ^2 value, but also on the change of the new fit obtained by excluding it. We also require the final fit to be stable to the further exclusion of indices (those that do not end up stable are GCs 45, 47 and 78). To achieve this it was often necessary to search for specific indices that destabilise the fit.

Indices that are excluded on this basis are in parentheses in Tables 2 and 3. On average, after all the exclusions, approximately 2/3 of the indices are used in the final fit. A major advantage of this method is that we are not reliant on Balmer indices (which can be contaminated by galaxy emission or strongly affected by BHBs). The errors given for the final derived parameters are statistical 1σ confidence intervals calculated by a Monte Carlo style method with 1000 realisations of the best-fit SSP.

4 DERIVED GC AGES, METALLICITIES AND ALPHA ABUNDANCES

The results of our fitting procedure are given in Table 4. We also present the metallicity estimates by the methods of BH90 and SB04. For GCs 45, 47 and 78, the SSP-derived parameters should be regarded with some caution as the final values are less reliable than those for the rest of the sample.

4.1 Age

The derived age for our sample are given in Table 4. All GCs have ages of greater than 10 Gyr; the only exception is GC38, with an inferred age of 8.9 Gyr. Our previous discussion of the effects of BHBs on age estimation in Section 3.2 leads us to suggest that GC38, with the strongest BHB

Table 4. Globular Cluster derived parameters. Age, $[\text{Fe}/\text{H}]_{SSP}$, $[\text{E}/\text{Fe}]$, $[\text{Z}/\text{H}]$, $[\text{Fe}/\text{H}]_{BH}$ and $[\text{Fe}/\text{H}]_{PCA}$ for the 16 GCs. Errors given are 1σ statistical errors, the PCA errors only include index errors and thus may be underestimates. Values in brackets indicate unreliable BH90 metallicity estimates.

ID	Age	$[\text{Fe}/\text{H}]_{SSP}$	$[\text{E}/\text{Fe}]$	$[\text{Z}/\text{H}]$	$[\text{Fe}/\text{H}]_{BH}$	$[\text{Fe}/\text{H}]_{PCA}$
GC	(Gyr)	(dex)	(dex)	(dex)	(dex)	(dex)
GC7	15.0±5.4	-1.27±0.18	0.34±0.16	-0.95±0.15	-1.54	-1.32±0.08
GC9	13.3±3.5	-0.74±0.13	0.15±0.10	-0.60±0.11	-0.68	-0.38±0.07
GC12	12.6±4.2	-0.63±0.12	0.38±0.09	-0.28±0.08	-0.49	-0.21±0.07
GC17	11.9±2.0	-1.58±0.23	0.32±0.22	-1.28±0.07	-1.39	-1.87±0.08
GC18	15.0±3.8	-0.65±0.11	0.34±0.08	-0.33±0.08	-0.58	-0.33±0.08
GC19	10.6±1.8	-1.38±0.22	0.06±0.22	-1.33±0.08	-1.34	-1.16±0.09
GC28	15.0±6.6	-0.81±0.21	0.12±0.13	-0.70±0.18	-0.90	-0.81±0.09
GC29	15.0±7.3	-1.15±0.23	0.27±0.13	-0.90±0.17	-1.15	-1.22±0.09
GC30	15.0±3.1	-0.63±0.11	0.30±0.07	-0.35±0.07	-0.29	-0.53±0.09
GC37	12.6±2.9	-1.42±0.19	0.34±0.17	-1.10±0.09	-1.03	-1.10±0.09
GC38	8.9±2.0	-2.05±0.17	0.50±0.07	-1.58±0.16	-1.36	-1.91±0.10
GC45	15.0±7.1	-2.38±0.46	0.80±0.37	-1.63±0.40	(-1.44)	-0.95±0.11
GC47	15.0±3.8	-0.24±0.12	0.15±0.06	-0.10±0.09	-0.54	-0.37±0.08
GC60	10.6±2.1	-2.27±0.24	0.50±0.19	-1.80±0.16	(-0.79)	-1.79±0.10
GC74	13.3±4.3	-2.08±0.42	0.30±0.41	-1.80±0.18	-1.62	-1.84±0.11
GC78	10.6±4.1	-0.70±0.21	0.03±0.14	-0.68±0.14	-1.31	-0.85±0.11

in our sample, is actually older than its inferred age. Assuming that the BHB in GC38 is stronger than modelled, then the true age and metallicity of this GC will be older and more metal-poor than given (although the BHB almost exclusively affects age-sensitive indices, age and metallicity are degenerate parameters in the SSP fitting process).

An index-index plot is presented in Figure 5 of $H\gamma_F$ vs $[\text{Fe}50\text{Mg}_1]$, where $[\text{Fe}50\text{Mg}_1] = \text{Fe}5015 \times \text{Mg}_1$. We have chosen this combination of Balmer and metal-sensitive lines as these indices appear to be the most accurate in our GC sample. The plot indicates that the GCs are consistent with being very old and covering a range of metallicity typical for GC systems. The GCs for which one of these two indices are not reliable, and hence not used in the best-fit solution, are also shown. These are GCs 45 and 47, for which $\text{Fe}5015$ and $H\gamma_F$ are affected by emission features in the index sidebands. These GCs have the most galactic background light due to their spatial positions (see Figure 2).

Figure 6 shows an age-metallicity plot for the GCs with values from Table 4. The GCs all have old ages for a large range in total metallicity ($[\text{Z}/\text{H}]$). The BHB GC38 has an arrow on it pointing in the direction corresponding to the age-metallicity 3:2 degeneracy (Worthey 1994).

4.2 Metallicity

A test of the reliability of the derived total metallicity $[\text{Z}/\text{H}]$ is obtained by plotting this measure against the empirical metallicity derived by the method of BH90 and that derived by the PCA method of SB04 (see Table 4). For the old

ages of these GCs both methods are well-calibrated. Figure 7 shows there is generally good agreement between the different methods over a metallicity range of ~ 2 dex. The PCA metallicities appear to show somewhat better agreement than those of BH90 with $[\text{Z}/\text{H}]$ derived from SSP models.

As a further consistency check of our results we plot the observed B–V colour from Forbes *et al.* (2001b) versus total metallicity $[\text{Z}/\text{H}]$ in Figure 7. We can see that the metallicity correlates well with the observed colour and is consistent with the 12 Gyr isochrone of the TMK04 SSP models with BHBs. We believe GC47 to have an anomalous colour (see discussion in the following paragraph).

Finally, we compare the observed colours of these GCs with colours predicted from the SSP derived ages and total metallicities. For GCs with $[\text{Z}/\text{H}] \leq -1$ we use the BHB mass loss models and for $[\text{Z}/\text{H}] > -1$ we use the RHB models with no mass loss. This is consistent with the HB morphology suggested by the CaII index values. The predicted colour errors are indicative estimates only. Figure 8 shows that there is reasonable agreement between the predicted and observed colour. The main outlier is GC47. The colours measured for GC47 disagree with its inferred age and metallicity. Also the spectra (see Figure 3) suggests that GC47 should have a colour similar to the reddest GC (i.e. GC12). Thus we suspect a systematic error in the observed colour for GC47.

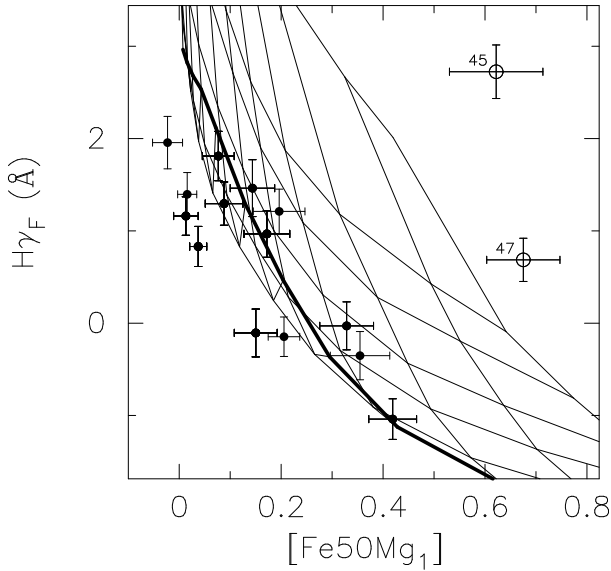


Figure 5. Index-index plot of $H\gamma_F$ vs $[Fe50Mg_1]$. Open circles indicate GCs for which one or more of the plotted indices are significantly affected by emission features in the index side-bands (i.e. GCs 45 and 47). Filled circles indicate GCs for which the three indices give fits similar to the full multi-index solution. The TMK04 grid lines shown are for $[E/Fe]=+0.3$ with metallicity in 0.25 dex steps from -2.25 to $+0.5$ (left to right) and ages of 1,2,3,5,8,12 and 15 Gyr (top to bottom), the heavier line is 15 Gyr. The GCs with reliable indices are consistent with old ages and a range of metallicities. Note that the ages used in this work are not derived from this plot.

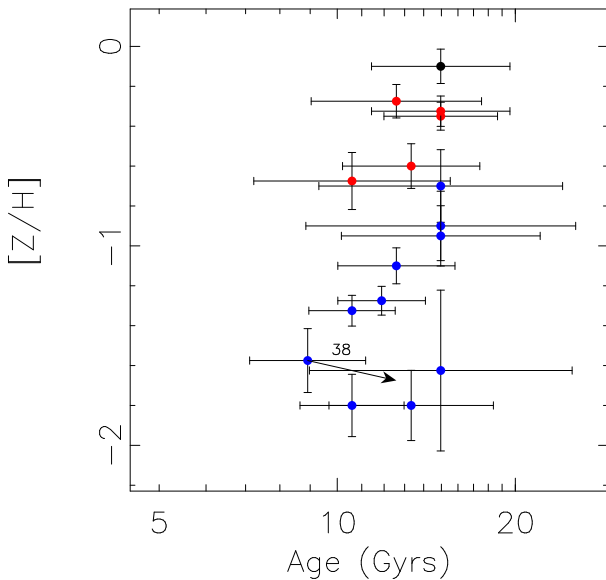


Figure 6. Age-metallicity distribution. The GCs are consistent with a coeval age of ~ 13 Gyr, and show a range of metallicities of ~ 2 dex. The arrow on GC38 indicates the direction it would shift towards assuming it is older than the SSP age indicates (due to the presence of a BHB artificially making it appear younger). In colour versions of this plot, the GCs are colour-coded according to their observed colour. The most metal-rich GC has an anomalously blue colour, otherwise the metal-poor GCs have blue colours and the metal-rich GCs are red.

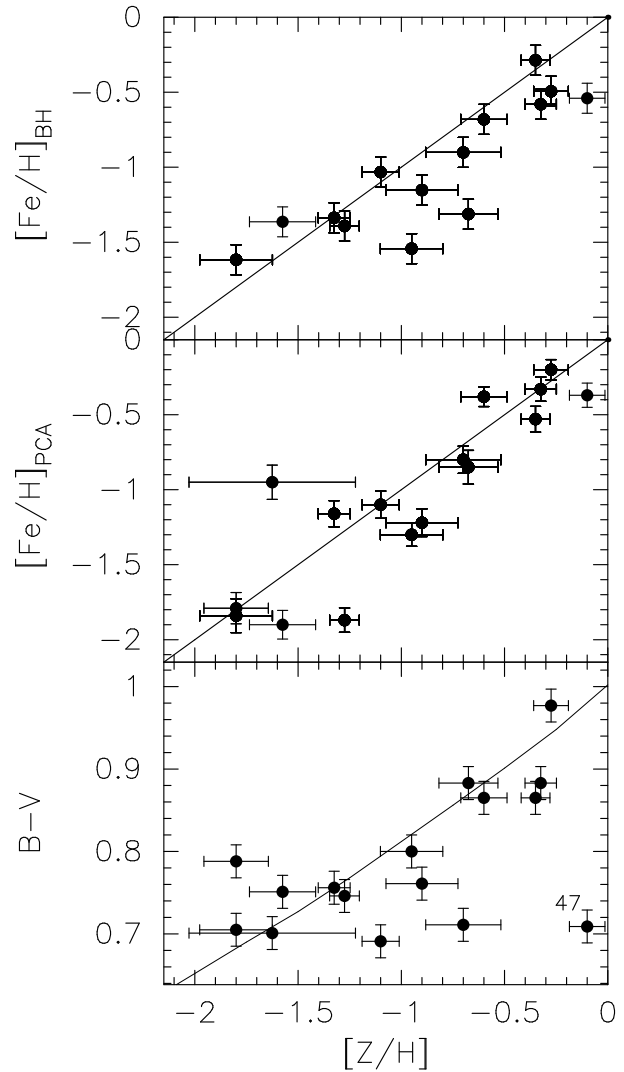


Figure 7. Comparison of empirical metallicities and observed colours with total metallicity. The top two plots show the metallicity from the method of BH90 ($[Fe/H]_{BH}$) and from SB04 ($[Fe/H]_{PCA}$). A one-to-one line is also shown. GCs 45 and 60 which have unreliable BH90 metallicities are not plotted. A good correlation is seen with points lying close to the one-to-one line for both empirical methods. The lower plot shows the observed $B-V$ colour from Forbes *et al.* (2001b) with $[Z/H]$. A reasonable agreement is found with the 12 Gyr isochrone from the TMK04 SSP models that include BHBs (solid line). The major outlier GC47 (which has an inexplicably blue colour) is labelled.

4.3 Abundance Ratio

We show relationship between $[E/Fe]$ and $[Fe/H]_{SSP}$ in Figure 9. The sum of these two measures approximates the total metallicity $[Z/H]$ ($[Fe/H]_{SSP}$ is derived from the fitted value of $[Z/H]$). The plot shows that $[E/Fe]$ is consistent with a value of twice solar ($[E/Fe]=+0.3$), except perhaps at the lowest metallicities ($[Fe/H]_{SSP} < -2$) where the extrapolation of the SSP model to high $[E/Fe]$ is becoming unreliable. Such values are similar to those found for Galactic GCs (e.g. Proctor *et al.* 2004).

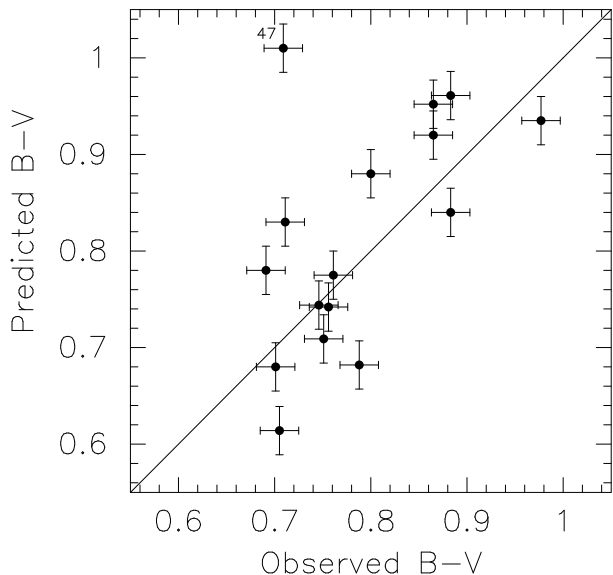


Figure 8. The B–V colour predicted from the inferred $[Z/H]$ and age is plotted against the observed B–V colour from Forbes *et al.* (2001b). The errors for the predicted colours are indicative only. GC47 which has an anomalous colour is labelled. For the other GCs there is good agreement between the predicted and observed colours.

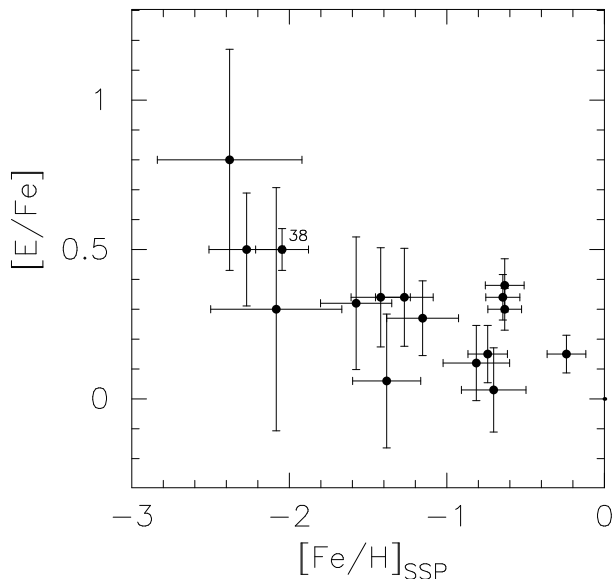


Figure 9. Abundance ratio against SSP derived iron metallicity. The GCs show a trend of decreasing $[E/Fe]$ with increasing $[Fe/H]_{SSP}$. However within errors a constant value of twice solar ($[E/Fe]=+0.3$) is consistent with the data.

5 GALAXY SPECTRUM

5.1 Long-slit Observations

On the same observing run (see Section 2) a 300s long-slit exposure along a P.A. = 60° centred on NGC 1052 itself was obtained. Standard reduction methods were used with IRAF software. Two dimensional distortions were measured on the arc lamp frames then removed using the task transform. The width for each aperture extracted increases with radius

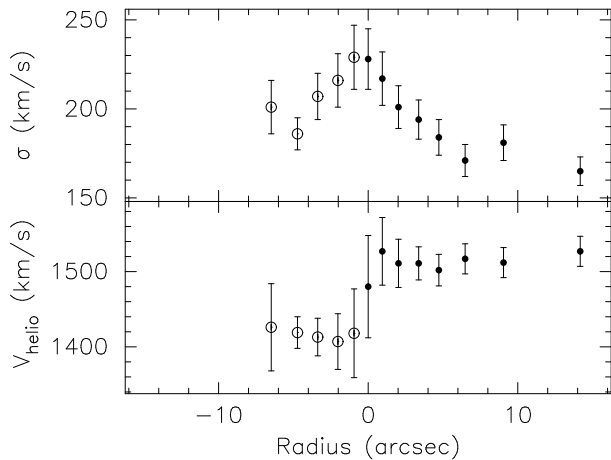


Figure 10. Recession velocity and velocity dispersion as functions of radius. Negative radii shown as open symbols indicate east-north-east of the galaxy centre, filled symbols indicate west-south-west. Rotation of order 50 km/s about the systemic velocity of 1470 km/s is clear from the lower panel. The velocity dispersion shown in the upper panel is peaked towards the galaxy centre.

to achieve a signal-to-noise of ~ 30 at 5000 Å for most of the apertures. The radial extent over which we can measure useful spectra is limited to $\sim 18''$ west-south-west of the galactic centre and $\sim 7.5''$ in the east-north-east direction.

For each spectrum, recession velocities were measured by cross-correlation using `fxcor` in IRAF. Velocity dispersions for the galaxy apertures were measured by cross-correlation with standard stars and comparison of the FWHM velocities with cross-correlations of the standard stars broadened by a range of velocity dispersions. This kinematic data is presented in Table 5.

5.2 Derived Parameters

Figure 10 shows that the galaxy rotates on the order of 50 km/s along our observed axis of P.A. = 60° . This rotation is consistent with that measured by Binney, Davies & Illingworth (1990), who find rotation of ~ 100 km/s along the major axis (P.A. = 120°) and none along the minor axis. Our observed axis is at an angle of 60° to the major-axis, therefore we expect the magnitude of rotation to be about $\cos(60^\circ)=0.5$ of that found along the major-axis as observed. The velocity dispersion is centrally peaked, with a maximum value of ~ 230 km/s, as found by Binney *et al.* (1990).

Lick indices were measured for the galaxy at each radius and the same offset to the Lick system was applied as per the GC data. Denicolo *et al.* (2005) presents indices, measured along the major axis of NGC 1052, which are consistent with our observed values. Several indices show gradients with galactocentric radius. A sample of these are plotted in Figure 11, showing some clear radial trends. The metallicity and $[E/Fe]$ sensitive indices (e.g., CN_2 and Mg_1) have a strong gradient towards higher values in the centre. A similar trend is observed for other $[E/Fe]$ sensitive indices, e.g., Mgb . The Fe5270 line, which is primarily sensitive to iron metallicity $[Fe/H]$, shows almost no gradient. Other Fe lines such as Fe4383, Fe4531 and Fe5406 also show no gradient with radius. These trends are also evident in the Denicolo

Table 5. Galaxy parameters. Radius is the centre of each aperture, where negative radii indicate east-north-east of the galaxy centre. 1σ errors are presented.

Radius (arcsec)	V_{helio} (km/s)	σ (km/s)	Age (Gyr)	[Fe/H] (dex)	[E/Fe] (dex)	[Z/H] (dex)
14.1	1527±20	165± 8	4.7±3.0	-0.08±0.22	0.42±0.07	0.32±0.21
9.1	1512±20	181±10	4.5±2.9	0.15±0.24	0.21±0.09	0.35±0.28
6.5	1517±20	171± 9	1.9±1.2	0.48±0.24	0.36±0.07	0.81±0.23
4.7	1502±21	184±10	1.8±0.9	0.65±0.17	0.42±0.06	1.05±0.19
3.4	1511±22	194±11	1.5±0.6	0.63±0.18	0.57±0.06	1.16±0.18
2.0	1511±32	201±12	2.1±1.0	0.65±0.13	0.51±0.05	1.13±0.15
1.0	1527±45	217±15	1.6±0.4	0.55±0.14	0.81±0.04	1.31±0.15
0.0	1480±68	228±17
-1.0	1418±59	229±18	1.8±0.4	0.65±0.11	0.84±0.05	1.44±0.12
-2.0	1407±37	216±15	1.6±0.4	0.65±0.11	0.69±0.04	1.30±0.12
-3.4	1413±25	207±13	1.9±0.7	0.63±0.13	0.51±0.05	1.11±0.15
-4.7	1419±21	186± 9	2.4±1.3	0.53±0.16	0.36±0.07	0.86±0.18
-6.5	1426±58	201±15	1.9±0.7	0.65±0.13	0.36±0.06	0.99±0.15

et al. (2005) data. The galaxy therefore posses strong gradients in [E/Fe] sensitive indices, but no gradients in the [Fe/H] sensitive indices. The effect of central galactic emission is obvious in the H β index plot, with large negative values at small radii. The other Balmer indices and Fe5015 are similarly affected by emission.

Due to the high total metallicity of the galaxy, we use the Fe– method from PS02 as opposed to the Trager *et al.* (2000a) method used earlier to calculate the [E/Fe]. This is necessary because the isochrone shape is driven by [Z/H] at low metallicity and [Fe/H] at high metallicity (see PS02 for a full explanation). Due to the high α -element abundance ratios present in the galaxy, we extrapolate the TMK04 models to [E/Fe]=+0.9. Figure 12 demonstrates the extremely high abundance ratios present in the central regions by showing a plot of $\langle \text{Fe} \rangle$ vs Mg b , where $\langle \text{Fe} \rangle = (\text{Fe}5270 + \text{Fe}5335)/2$.

To obtain reasonable fits to the TMK04 SSP models it was necessary to exclude several indices from all apertures during the fitting process. Galactic emission which increases towards the centre, forces the removal of all the Balmer lines and Fe5015 from the fitting process. The index C4668 was also removed due to its systematic deviance from the best fit.

We also clipped individual deviant indices following a similar method to Section 3.3. This resulted in a total of 12% of the remaining indices being removed (mostly Mg $_2$, Ca4455 and Fe4383). We were unable to obtain reasonable fits for the central aperture, probably due to strong galactic emission, and do not present the fitted parameters for it. The values obtained for age, [Fe/H], [E/Fe] and [Z/H] are presented in Table 5 and also plotted against radius in Figure 13.

Figure 13 shows no strong radial gradient in either age or [Fe/H]. There is however a very strong gradient of decreas-

ing [E/Fe] with increasing radius. In the central arcsecond the estimated [E/Fe] of $\sim +0.8$ dex is unusually high.

6 GLOBULAR CLUSTER KINEMATICS

Using the kinematic information from the 16 GCs, we can estimate the mass enclosed within the radius of the GC system observed. We use the projected mass estimator (Evans *et al.* 2003), assuming isotropy and an r^{-4} distribution to derive a mass of $1.7 \pm 0.9 \times 10^{12} M_{\odot}$ within 19 kpc ($\sim 6.5 r_e$). The mass estimate error was calculated by bootstrapping the observed velocities and errors. van Gorkom *et al.* (1986) used HI kinematics to measure a mass of $3.1 \times 10^{11} M_{\odot}$ within 23 kpc. We have limited spatial coverage and too few GCs to make any comment on systematic rotation of the GC system. Since our mass estimate is significantly higher than that for the HI kinematics, our assumption of isotropy may be incorrect. For example, if the orbits had a rather strong tangential bias of $\sigma_t/\sigma_r = 2$, then our tracer mass estimate would be 30% too large (Evans *et al.* 2003).

7 DISCUSSION

To summarise, we have obtained spectra for 16 GCs which sample both the blue and red sub-populations in NGC 1052. Ages, metallicities and abundance ratios for these GCs have been derived using the multi-line fitting technique of PS02 applied to the SSPs of TMK04. We find that the blue GCs in NGC 1052 to be uniformly old ≥ 10 Gyr and metal-poor (with the exception of GC47 for which we strongly suspect an incorrect colour). The red GCs are similarly old but metal-rich. We do not find any young GCs associated

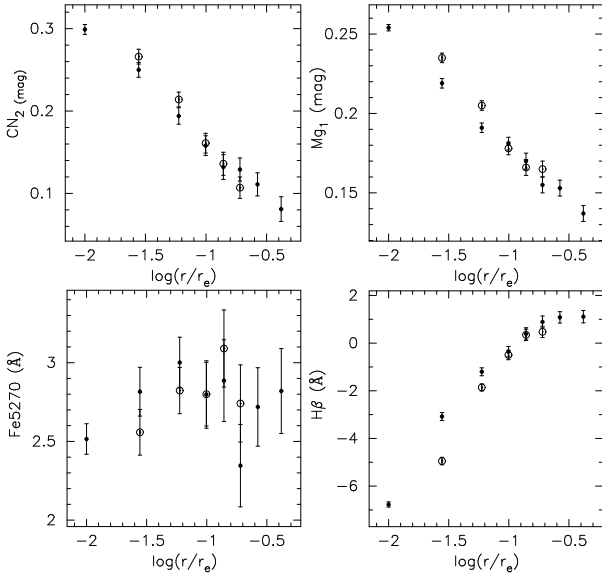


Figure 11. Representative plots of indices vs. \log radius in terms of the effective radius ($r_e=34''$). We have folded the data about the centre with points from the east-north-east marked with open symbols, filled symbols indicate west-south-west. The strong emission in $H\beta$ is clearly seen as negative values. This highlights the need to exclude the Balmer indices from our fitting process. The Mg_1 gradient when viewed in tandem with the Fe5270 lack of gradient implies that $[Fe/H]$ is roughly constant with radius and that the abundance ratio is much greater in the central region. The gradient in other α -element sensitive indices reinforces this picture.

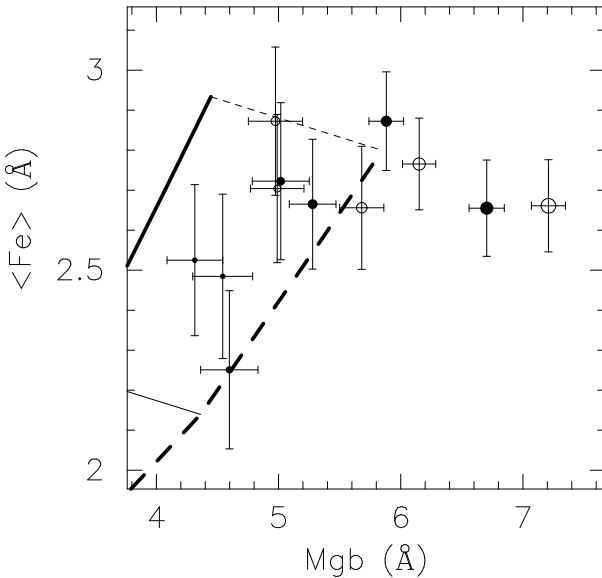


Figure 12. Plot of $\langle Fe \rangle$ vs Mgb indices. Bold lines shown the 2 Gyr isochrones of $[E/Fe]=+0.3$ dex (solid) and $[E/Fe]=+0.6$ dex (dashed). The thin lines show $[Fe/H]=+0.0$ (solid) and $+0.4$ (dashed). Point sizes decrease with radius. The open symbols are the east-north-east apertures and the filled symbols indicate the apertures towards the west-south-west. The plot shows that the central apertures are the most α -element enhanced with abundance ratios above $+0.6$ dex.

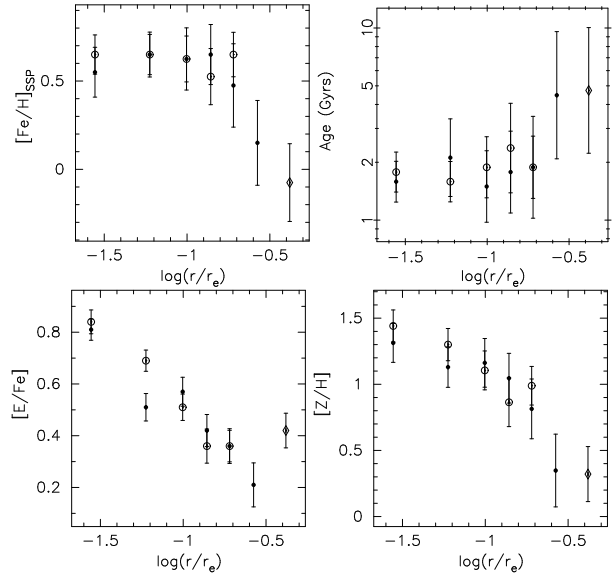


Figure 13. The derived stellar population parameters for the galaxy field stars are plotted with radius. We have folded the data about the galaxy centre with points from the east-north-east marked with open circles, filled symbols indicate west-south-west. The open diamond indicates the aperture which has a less reliable fit. The central galaxy aperture is not shown. There is no strong gradient in either age or iron metallicity. There is a clear trend of α -element abundance ratio increasing towards the centre. Total metallicity shows a radial gradient.

with the recent merger event, even though we have sampled the expected colour and luminosity regime for young GCs.

We do, however find evidence for young *galaxy* stars associated with the merger event. Our luminosity-weighted age of ~ 2 Gyr for the NGC 1052 stars is compatible with that estimated from the HI tidal tails and infalling HI gas of ~ 1 Gyr (van Gorkom *et al.* 1986).

The high central value and strong gradient observed for $[E/Fe]$ in NGC 1052 is unusual for an elliptical galaxy. For example, Mehlert *et al.* (2003) find negligible gradients in $[E/Fe]$ for 35 early-type galaxies in their sample of Coma galaxies. Proctor (2002) using the same method as this work finds a maximum $[E/Fe] \simeq +0.4$ and no significant $[E/Fe]$ gradient in the bulges of 28 late and early-type galaxies.

The α -element abundance ratio for NGC 1052 is largely insensitive to the combination of indices we fit, unlike age and metallicity. Therefore, barring a major contamination of all the $[E/Fe]$ sensitive indices (which must also affect the observations of Denicolo *et al.* 2005) we can confidently say that the central galaxy starlight is more α -element enhanced than $\sim +0.6$ dex. Such α -element enhancements and the deduced high central metallicities ($[Z/H]=+1.3$ dex) are far beyond current SSP models. Therefore, it is impossible to pin down exact values for the central galaxy field stars. At $[Z/H]=+1.3$ the total metallicity would be 20 times that of the Sun, implying a metal content by mass of $\sim 40\%$. This value is unrealistically high, which suggesting that our extrapolations beyond the current SSP models are unreliable.

van Gorkom *et al.* (1986) speculated that NGC 1052 had accreted a gas-rich dwarf galaxy about 1 Gyr ago. They find a total HI mass of $\sim 5 \times 10^8 M_\odot$ which seems consistent with this idea. Such a small quantity of gas could also explain

why we have detected no GCs forming in this merger (even allowing for some cold gas to have been used up in field star formation and/or ionised). Even a small burst by mass will give a young age for the galaxy central stars (Terlevich & Forbes 2002).

Our results also indicate that the central merger-induced starburst involved very high metallicity and α -element enhanced gas. Such high metallicity gas is not usually associated with dwarf galaxies but massive spirals. The most obvious explanation for the high α -element enhancement is a high central concentration Type II supernovae from the starburst. Inflows over any significant timescale are less likely, since no radial metallicity gradient is seen. A spiral galaxy with a small bulge and on-going star formation in the disk could produce the young central ages observed without star formation from the merger itself being the dominant luminosity source.

To better evaluate these possibilities we need stellar population information for the galaxy out to at least one effective radius. This will provide an age, metallicity and α -element abundance ratio for the assumed old (>10 Gyr) underlying population. With this information the next step would be to apply a chemo-gas code in an attempt to reproduce the observed properties.

In terms of the GC formation models described in the Introduction, the detection of old red and blue GC sub-populations in NGC 1052 is generally consistent with the predictions of both Forbes *et al.* (1997) and Cote *et al.* (1998). The ages are not yet accurate enough to determine whether the red GCs are a few Gyr younger than the blue ones as expected in Forbes *et al.* (1997). On the other hand, we find no evidence for GCs forming in the merger event, in contrast to the expectations of the merger model of Ashman & Zepf (1992).

There are now several examples of galaxies with spectroscopically confirmed *minor* contributions to their GC systems from recently formed GCs, while the vast bulk of their GCs appear to be very old. NGC 1399, a central cluster galaxy which is old and has no photometric indication of intermediate-age GCs, may have a small number of ~ 2 Gyr old GCs (Forbes *et al.* 2001a). Photometry of GCs in the merger remnant NGC 3610, which has a spectroscopic age of 1.6 ± 0.5 Gyrs (Denicolo *et al.* 2005), suggested the presence of an intermediate-age sub-population (Whitmore *et al.* 2002). However, spectroscopy of some of these candidate intermediate-age GCs indicates that only a small portion of these clusters are in fact ~ 2 Gyr old (Strader *et al.* 2004).

Perhaps the best example of intermediate-age GCs in a merger remnant is NGC 1316, it has a similar age (~ 3 Gyrs) and lies at a similar distance (22.9 Mpc) to NGC 1052 (Goudfrooij *et al.* 2001). Figure 14 shows a comparison of the colour magnitude diagrams for the spectroscopically confirmed GCs of these two galaxies. Only the 3 brightest NGC 1316 GCs had high enough S/N to measure ages, and these are 2 magnitudes brighter in V than the brightest GCs for which we obtained spectra in NGC 1052. All three GCs were found to be ~ 3 Gyrs old and solar metallicity (Goudfrooij *et al.* 2001). The NGC 1316 GC colour distribution peaks at $B-I \sim 1.8$, which lies between the peaks of the NGC 1052 GC colour distribution. There is no significant population of NGC 1052 GCs in the same colour and magnitude parameter space as the young NGC 1316 GCs.

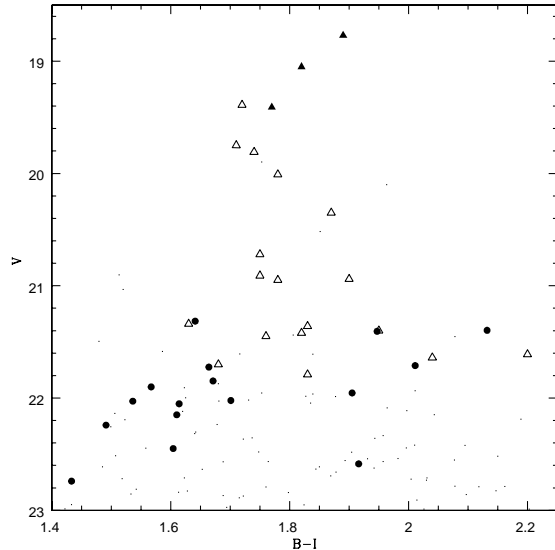


Figure 14. The colour magnitude diagram for spectroscopically confirmed GCs around NGC 1052 (filled circles). The small dots are GC candidates around NGC 1052 from the imaging of Forbes *et al.* (2001b). The triangles are spectroscopically confirmed GCs around NGC 1316 (Goudfrooij *et al.* 2001) with their magnitude's adjusted to account for the distance modulus difference. Only the filled triangles had high enough S/N for ages and metallicities to be measured, the open triangles have measured velocities but not indices. Most of the NGC 1316 GCs have intermediate colours ($B-I \sim 1.8$) and are significantly brighter than the NGC 1052 GCs. Therefore we do not expect a similar sub-population of ~ 3 Gyr GCs in NGC 1052.

Therefore we do not expect a similar sub-population of ≤ 3 Gyr GCs in NGC 1052.

8 CONCLUSIONS

We have obtained low-resolution spectra for 19 Globular Cluster (GC) candidates associated with the merger remnant elliptical NGC 1052. Of this sample, 16 are identified as *bona fide* GCs by their radial velocities. Using these velocities, we derive a virial mass of $1.7 \pm 0.9 \times 10^{12} M_{\odot}$ within a radius of $\sim 6.5 r_e$ (19 kpc). If the orbits had a strong tangential bias then our tracer mass estimate would be 30% too large.

Using the multi-index χ^2 fitting technique of Proctor & Sansom (2002), and the simple stellar population models of Thomas, Maraston & Korn (2004) we derive individual ages, metallicities and abundance ratios for the 16 confirmed GCs. We find all of the GCs to be very old, i.e. ≥ 10 Gyr, with a range of metallicities. The predicted colours, based on the derived ages and metallicities, agree well with the observed GC colours. We find no evidence for young GCs associated with the likely minor merger event ~ 1 Gyr ago.

We also obtained a long-slit spectrum covering the central $\sim 15''$ of NGC 1052. No strong gradient in either age or metallicity was found. However, a large abundance ratio gradient exists. The stellar population in the central regions of NGC 1052 has a luminosity-weighted age of ~ 2 Gyr with

[Fe/H] $\sim +0.6$ and a very high α -element abundance ratio of $\sim +0.8$ dex. The recent central star formation episode was most likely induced by infalling gas associated with the recent merger. Thus, although NGC 1052 shows substantial evidence for a recent merger and an associated starburst, it appears that the merger did not induce the formation of many, if any, new GCs. As the formation of luminous star clusters appears to accompany most significant star formation events, the absence of young GCs and the high [E/Fe] values in the center of the galaxy (suggesting short star formation timescales) may indicate that a relatively small amount of star formation occurred in the merger. This interpretation is consistent with “frosting” models for the formation of early-type galaxies (e.g., Trager *et al.* 2000b).

9 ACKNOWLEDGMENTS

We thank Soeren Larsen for help preparing the slit mask. Part of this research was funded by NSF grant AST-02-06139. The data presented herein were obtained at the W.M. Keck Observatory, which is operated as a scientific partnership among the California Institute of Technology, the University of California and the National Aeronautics and Space Administration. The Observatory was made possible by the generous financial support of the W.M. Keck Foundation. This research has made use of the NASA/IPAC Extragalactic Database (NED), which is operated by the Jet Propulsion Laboratory, Caltech, under contract with the National Aeronautics and Space Administration. DF and RP thanks the ARC for their financial support.

REFERENCES

- Ashman, K.M., Zepf, S.E., 1992, *ApJ*, 384, 50
 Beasley, M.A., Baugh, C.M., Forbes, D.A., Sharples, R.M., Frenk, C.S., 2002, *MNRAS*, 333, 383
 Beasley, M. A., Brodie, J.P., Strader, J., Forbes, D.A., Proctor, R.N., Barmby, P., Huchra, J.P., 2004, *AJ*, 128, 1623
 Binney, J.J., Davies, R.L., Illingworth, G.D., 1990, *ApJ*, 361, 78
 Brodie, J.P., Huchra J.P., 1990, *ApJ*, 362, 503
 Bruzual, A. G., Charlot, S., 2003, *MNRAS*, 344, 1000
 Cote, P., Marzke, R. O., West, M. J., 1998, *ApJ*, 501, 554
 Davies, R.L., Kuntschner, H., Emsellem, E., Bacon, R., Bureau, M., Carollo, C.M., Copin, Y., Miller, B.W., Monnet, G., Peletier, R.F., Verolme, E.K., de Zeeuw, P.T., 2001, *ApJ*, 548, 1, L33
 Denicolo, G., Terlevich, R., Terlevich, E., Forbes, D., Terlevich, A., Carrasco, L., 2005, *MNRAS*, 356, 1440
 Evans, N.W., Wilkinson, M.I., Perrett, K.M., Bridges, T.J., 2003, *ApJ*, 583, 752
 Forbes, D.A., Beasley, M.A., Brodie, J.P., Kissler-Patig, M., 2001a *ApJ*, 563, 143
 Forbes, D. A., Brodie, J. P., Grillmair, C. J., 1997, *AJ*, 113, 1652
 Forbes, D.A., Georgakakis, A. E., Brodie, J.P., 2001b, *MNRAS*, 325, 1431
 Forbes, D.A., Ponman, T.J., Brown, R.J.N., 1998, *ApJ*, 508, L43
 Forbes, D.A., Sparks, W., Macchetto, F.D., 1990, In *Paired and Interacting Galaxies*, p 431, ed J. Sulentic, W. Keel, C. Tele-sco, NASA.
 Goudfrooij P., Mack, J., Kissler-Patig, M., Meylan, G., Minniti, D., 2001, *MNRAS*, 322, 643
 Harris, W. E., 2001, in Saas-Fee Advanced School on Star Clusters, ed. L. Labhardt & B. Binggeli (course 28) (New York: Springer)
 Kuntschner, H., Ziegler, B.L., Sharples, R.M., Worthey, G., Fricke, K.J., 2002, *A&A*, 395, 761
 Larsen, S.S., Brodie, J.P., Beasley, M.A., Forbes, D.A., Kissler-Patig, M., Kuntschner, H., Puzia, T.H., 2003, *ApJ*, 585, 767
 Lee, H.-C., Yoon, S.-J., Lee, Y.-W., 2000, *AJ*, 120, 998
 Maraston, C., Greggio, L., Thomas, D., 2001a, *Ap&SS*, 276, 893
 Maraston, C., Kissler-Patig, M., Brodie, J. P., Barmby, P., Huchra, J. P., 2001b, *A&A*, 370, 176
 Mehlert, D., Thomas, D., Saglia, R.P., Bender, R., Wegner, G., 2003, *A&A*, 407, 423
 Miller, B.W., Whitmore, B.C., Schweizer, F., Fall, S.M., 1997, *AJ*, 14, 2381
 Oke, J. B., Cohen, J. G., Carr, M., Cromer, J., Dingizian, A., Harris, F., H. Labrecque, S., Lucinio, R., Schaal, W., Epps, H., Miller, J., 1995, *PASP*, 107, 375
 Plana, H., Boulesteix, J., 1996, *A&A*, 307, 391
 Proctor, R.N., 2002, Ph. D. Thesis, University of Central Lancashire, UK
 Proctor, R.N., Sansom, A.E., 2002, *MNRAS*, 333, 517
 Proctor, R.N., Forbes, D.A., Beasley, M.A., 2004, *MNRAS*, 355, 1327
 Prugniel, P., Simien, F., 1996, *A&A*, 309, 749
 Rich, R. M., et al., 1997, *ApJL*, 484, L25
 Rose, J. A., 1984, *AJ*, 89, 1238
 Schiavon, R. P., Rose, J. A., Courteau, S., & MacArthur, L. 2004, *ApJL*, 608, L33
 Schweizer, F., Seitzer, P., 1992, *AJ*, 104, 1039
 Schweizer, F., Seitzer, P., 1998, *AJ*, 116, 2206
 Schweizer, F., Seitzer, P., Brodie, J.P., 2004, *AJ*, 128, 202
 Schweizer, F., Miller, B.W., Whitmore, B.C., Fall, S.M., 1996, *AJ*, 112, 1839
 Strader, J., Brodie, J.P., 2004, *AJ*, in press, astro-ph/0407001
 Strader, J., Brodie, J.P., Forbes, D.A., 2004, *AJ*, 127, 295
 Strader, J., Brodie, J.P., Schweizer, F., Larsen, S.S., Seitzer, P., 2003, *AJ*, 125, 626
 Terlevich, A.I., Forbes, D.A., 2002, *MNRAS*, 330, 547
 Trager, S. C., Faber, S. M., Worthey, G., Gonzarlez, J. J., 2000a, *AJ*, 119, 1645
 Trager, S. C., Faber, S. M., Worthey, G., Gonzarlez, J. J., 2000b, *AJ*, 120, 165
 Trager, S. C., Worthey, G., Faber, S. M., Burstein, D., Gonzarlez, J. J., 1998, *ApJS*, 116, 1
 Thomas, D., Maraston, C., Bender, R., 2003, *MNRAS*, 339, 897
 Thomas, D., Maraston, C., Korn, A., 2004, *MNRAS*, 351, 19
 Trippico, M.J., 1989, *AJ*, 97, 735
 Van Gorkom, J.H., Knapp, G.R., Raimond, E., Faber, S.M., Gal-lagher, J.S., 1986, *AJ*, 91, 791
 Van Gorkom, J.H., Knapp, G.R., Ekers, R.D., Ekers, D.D., Laing, R.A., Polk, K.S., 1989, *AJ*, 97, 708
 Vazdekis, A., 1999, *ApJ*, 513, 224
 Worthey, G., 1994, *ApJS*, 95, 107
 Worthey, G., Ottaviani, D.L., 1997, *ApJS*, 111, 377
 Whitmore, B. C., Schweizer, F., 1995, *AJ*, 109, 960
 Whitmore, B.C., Schweizer, F., Kundu, A., Miller, B., 2002, *AJ*, 124, 147